Deep inelastic scattering

This chapter describes high-energy electron—proton inelastic scattering where the proton breaks up in the interaction. The inelastic scattering process is first discussed in terms of a general Lorentz-invariant extension of the ideas introduced in the previous chapter, with form factors replaced by structure functions. Deep inelastic scattering is then described by the QED interaction of a virtual photon with the constituent quarks inside the proton. The experimental data are then interpreted in the quark—parton model and the measured structure functions are related to parton distribution functions that describe the momentum distributions of the quarks. From the experimental measurements, the proton is found to be a complex dynamical system comprised of quarks, gluons and antiquarks.

8.1 Electron-proton inelastic scattering

Because of the finite size of the proton, the cross section for electron–proton elastic scattering decreases rapidly with energy. Consequently, high-energy e⁻p interactions are dominated by inelastic scattering processes where the proton breaks up. For e⁻p \rightarrow e⁻X inelastic scattering, shown in Figure 8.1, the hadronic final state resulting from the break-up of the proton usually consists of many particles. The invariant mass of this hadronic system, denoted W, depends on the four-momentum of the virtual photon, $W^2 = p_4^2 = (p_2 + q)^2$, and therefore can take a range of values. Compared to the elastic scattering process, where the invariant mass of the final state is always the mass of the proton, this additional degree of freedom in the inelastic scattering process means that the event kinematics must be specified by two quantities. Whereas e⁻p \rightarrow e⁻p elastic scattering was described in terms of the electron scattering angle alone, the two kinematic variables used to describe inelastic scattering are usually chosen from the Lorentz-invariant quantities W, x, y, v and Q^2 , defined below.

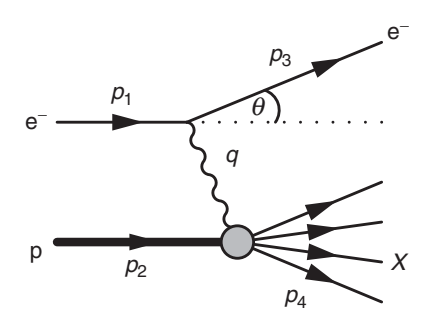


Fig. 8.1 Electron—proton inelastic scattering.

8.1.1 Kinematic variables for inelastic scattering

As was the case for elastic scattering, Q^2 is defined as the negative four-momentum squared of the virtual photon,

$$Q^2 = -q^2.$$

When written in terms of the four-momenta of the initial- and final-state electrons,

$$Q^2 = -(p_1 - p_3)^2 = -2m_e^2 + 2p_1 \cdot p_3 = -2m_e^2 + 2E_1E_3 - 2p_1p_3\cos\theta.$$

In inelastic scattering, the energies are sufficiently high that the electron mass can be neglected and therefore, to a very good approximation

$$Q^2 \approx 2E_1 E_3 (1 - \cos \theta) = 4E_1 E_3 \sin^2 \frac{\theta}{2},$$

implying that Q^2 is always positive.

Bjorken x

The Lorentz-invariant dimensionless quantity

$$x \equiv \frac{Q^2}{2p_2 \cdot q},\tag{8.1}$$

will turn out to be an important kinematic variable in the discussion of the quark model of deep inelastic scattering. The range of possible values of x can be found by writing the four-momentum of the hadronic system in terms of that of the virtual photon

$$W^2 \equiv p_4^2 = (q + p_2)^2 = q^2 + 2p_2 \cdot q + p_2^2$$

$$\Rightarrow W^2 + Q^2 - m_p^2 = 2p_2 \cdot q,$$

and therefore, from the definition of (8.1),

$$x = \frac{Q^2}{Q^2 + W^2 - m_{\rm p}^2}. (8.2)$$

Because there are three valence quarks in the proton, and quarks and antiquarks can be produced together only in pairs, the hadronic final state in an e⁻p inelastic scattering process must include at least one baryon (qqq). Consequently, the invariant mass of the final-state hadronic system is always greater than the mass of the proton (which is the lightest baryon), thus

$$W^2 \equiv p_4^2 \ge m_{\rm p}^2.$$

Because $Q^2 \ge 0$ and $W^2 \ge m_p$, the relation of (8.2) implies that x is always in the range

$$0 \le x \le 1$$
.

The value of x expresses the "elasticity" of the scattering process. The extreme case of x = 1 is equivalent to $W^2 = m_p^2$, and therefore corresponds to elastic scattering.

y and ν

A second dimensionless Lorentz-invariant quantity, the inelasticity y, is defined as

$$y \equiv \frac{p_2 \cdot q}{p_2 \cdot p_1}.$$

In the frame where the proton is at rest, $p_2 = (m_p, 0, 0, 0)$, the momenta of the initial-state e^- , the final-state e^- and the virtual photon can be written

$$p_1 = (E_1, 0, 0, E_1), p_3 = (E_3, E_3 \sin \theta, 0, E_3 \cos \theta) \text{ and } q = (E_1 - E_3, \mathbf{p}_1 - \mathbf{p}_3),$$

and therefore

$$y = \frac{m_{\rm p}(E_1 - E_3)}{m_{\rm p}E_1} = 1 - \frac{E_3}{E_1}.$$
 (8.3)

Hence y can be identified as the fractional energy lost by the electron in the scattering process in the frame where the proton is initially at rest. In this frame, the energy of the final-state hadronic system is always greater than the energy of the initial-state proton, $E_4 \ge m_p$, which implies the electron must lose energy. Consequently, y is constrained to be in the range

$$0 \le y \le 1$$
.

Sometimes it is more convenient to work in terms of energies, rather than the fractional energy loss described by y. In this case the related quantity

$$v \equiv \frac{p_2 \cdot q}{m_{\rm p}},\tag{8.4}$$

is often used. In the frame where the initial-state proton is at rest,

$$\nu = E_1 - E_3,$$

is simply the energy lost by the electron.

Relationships between kinematic variables

For a given centre-of-mass energy \sqrt{s} , the kinematics of inelastic scattering are fully defined by specifying two independent observables which are usually chosen to be two of Lorentz-invariant quantities, Q^2 , x, y and v. Provided the chosen quantities are independent, the other two quantities then can be determined through the relations that follow from the definitions,

$$Q^2 \equiv -q^2$$
, $x \equiv \frac{Q^2}{2p_2 \cdot q}$, $y \equiv \frac{p_2 \cdot q}{p_2 \cdot p_1}$ and $v \equiv \frac{p_2 \cdot q}{m_p}$. (8.5)

For example, it immediately can be seen that x is related to Q^2 and ν by

$$x = \frac{Q^2}{2m_p \nu}. ag{8.6}$$

Furthermore, for a fixed centre-of-mass energy,

$$s = (p_1 + p_2)^2 = p_1^2 + p_2^2 + 2p_1 \cdot p_2 = 2p_1 \cdot p_2 + m_p^2 + m_e^2$$

Since $m_e^2 \ll m_p^2$, to a good approximation

$$2p_1\cdot p_2\simeq s-m_{\rm p}^2,$$

and then from the definitions of (8.5), it follows that y is proportional to ν ,

$$y = \left(\frac{2m_{\rm p}}{s - m_{\rm p}^2}\right)\nu. \tag{8.7}$$

Finally from (8.6) and (8.7), it can be seen that Q^2 is related to x and y by

$$Q^2 = (s - m_p^2)xy. (8.8)$$

Hence, for a fixed centre-of-mass energy, the kinematics of inelastic scattering can be described by any two of the Lorentz-invariant quantities x, Q^2 , y and v, with the exception of y and v, which are not independent.

Fig. 8.2

8.1.2 Inelastic scattering at low Q^2

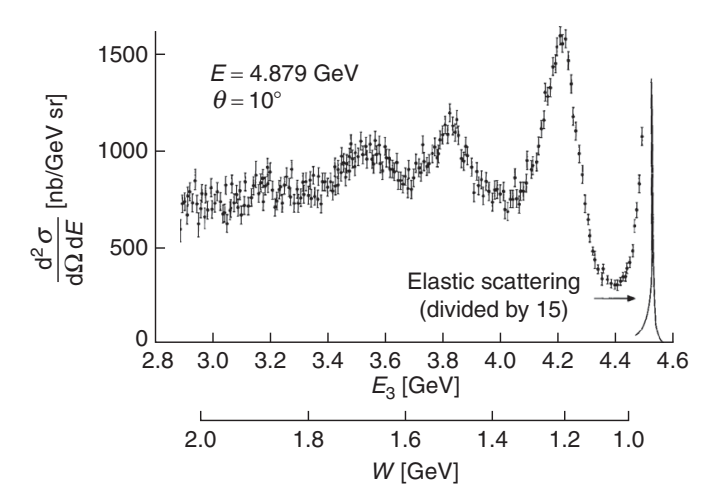
For electron–proton scattering at relatively low electron energies, both elastic and inelastic scattering processes can occur. For example, Figure 8.2 shows the observed energy distribution of electrons scattered through an angle of $\theta = 10^{\circ}$ at a fixed-target experiment at DESY, where electrons of energy $E_1 = 4.879 \,\text{GeV}$ were fired at a liquid hydrogen target (essentially protons at rest). Because two independent variables are required to define the kinematics of inelastic scattering, the corresponding *double-differential* cross section is expressed in terms of two variables, in this case $d^2\sigma/d\Omega \,dE_3$.

Since the kinematics of an individual interaction are fully specified by two independent variables, in this case the angle and energy of the scattered electron, θ and E_3 , the invariant mass W of the unobserved final-state hadronic system can be determined on an event-by-event basis using

$$W^{2} = (p_{2} + q)^{2} = p_{2}^{2} + 2p_{2} \cdot q + q^{2} = m_{p}^{2} + 2p_{2} \cdot (p_{1} - p_{3}) + (p_{1} - p_{3})^{2}$$

$$\approx \left[m_{p}^{2} + 2m_{p}E_{1} \right] - 2 \left[m_{p} + E_{1}(1 - \cos\theta) \right] E_{3}.$$
(8.9)

Hence, for electrons detected at a fixed scattering angle, the invariant mass W of the hadronic system is linearly related to the energy E_3 of the scattered electron. Consequently the energy distribution of Figure 8.2 can be interpreted in terms of W. The large peak at final-state electron energies of approximately 4.5 GeV corresponds to $W = m_p$, and these electrons can be identified as coming from elastic scattering. The peak at $E_3 \approx 4.2$ GeV corresponds to resonant production of a single Δ^+ baryon with mass W = 1.232 GeV (see Chapter 9). The two smaller peaks at $E_3 \sim 3.85$ GeV and $E_3 \sim 3.55$ GeV correspond to resonant production of other



The energy of the scattered electron in low-energy electron—proton scattering and the corresponding invariant mass *W* of the final state hadronic system. From Bartel *et al*. (1968).

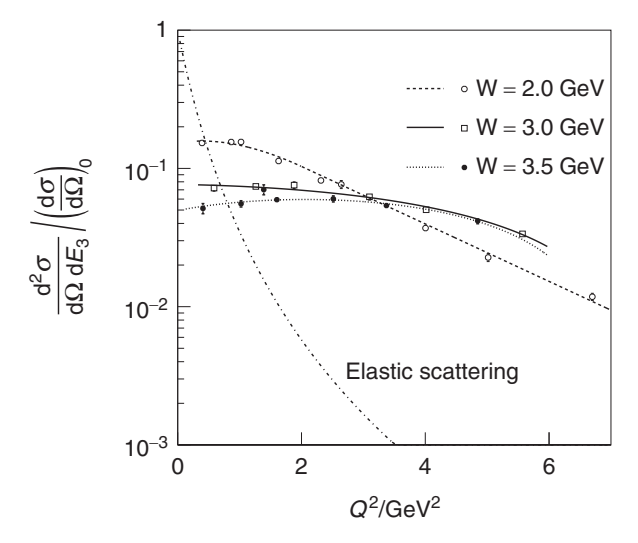


Fig. 8.3 Low- Q^2 measurements of the electron—proton inelastic scattering cross section scaled to the Mott cross section. Also shown is the expected dependence for elastic scattering. Adapted from Breidenbach *et al.* (1969).

baryon states. These resonances are essentially excited bound states of the proton (uud), which subsequently decay strongly, for example $\Delta^+ \to p\pi^0$. The full-width-at-half-maximum (FWHM) of a resonance as a function of W is equal to the total decay rate Γ , which in turn is related to the lifetime of the resonant state by $\Gamma = 1/\tau$. The continuum at higher W is the start of the *deep inelastic* region where the proton is broken up in the collision, resulting in multi-particle final states.

Figure 8.3 shows measurements of the $e^-p \to e^-X$ differential cross section scaled to the Mott scattering cross section of (7.36). The data are plotted as function of Q^2 for three different values of W. The expected ratio for elastic scattering, assuming the dipole form for $G_E(Q^2)$ and $G_M(Q^2)$ is shown for comparison. The inelastic cross sections are observed to depend only weakly on Q^2 , in contrast to rapidly falling elastic scattering cross section. In the deep inelastic region (higher values of W), the near Q^2 independence of the cross section implies a constant form factor, from which it can be concluded that deep inelastic scattering occurs from point-like (or at least very small) entities within the proton.

8.2 Deep inelastic scattering

The most general Lorentz-invariant form of the $e^-p \rightarrow e^-p$ elastic scattering cross section from the exchange of a single photon is given by the Rosenbluth formula of (7.33),

$$\frac{d\sigma}{d\Omega} = \frac{\alpha^2}{4E_1^2 \sin^4(\theta/2)} \frac{E_3}{E_1} \left(\frac{G_E^2 + \tau G_M^2}{(1+\tau)} \cos^2 \frac{\theta}{2} + 2\tau G_M^2 \sin^2 \frac{\theta}{2} \right).$$

This can be expressed in an explicitly Lorentz-invariant form using the definitions of Q^2 and y (see Problem 8.2):

$$\frac{\mathrm{d}\sigma}{\mathrm{d}Q^2} = \frac{4\pi\alpha^2}{Q^4} \left[\frac{G_E^2 + \tau G_M^2}{(1+\tau)} \left(1 - y - \frac{m_\mathrm{p}^2 y^2}{Q^2}\right) + \frac{1}{2} y^2 G_M^2 \right].$$

The Q^2 dependence of the form factors $G_E(Q^2)$ and $G_M(Q^2)$ and $\tau = Q^2/4m_p$ can be absorbed into two new functions, here written as $f_1(Q^2)$ and $f_2(Q^2)$, such that

$$\frac{d\sigma}{dQ^2} = \frac{4\pi\alpha^2}{Q^4} \left[\left(1 - y - \frac{m_p^2 y^2}{Q^2} \right) f_2(Q^2) + \frac{1}{2} y^2 f_1(Q^2) \right]. \tag{8.10}$$

Although y appears in this formula, it should be remembered that for elastic scattering x = 1 and therefore y is a function of Q^2 alone. In this form, $f_1(Q^2)$ is associated with the purely magnetic interaction and $f_2(Q^2)$ has electric and magnetic contributions.

8.2.1 Structure functions

Equation (8.10) can be generalised to the inelastic scattering process, where the differential cross section has to be expressed in terms of two independent kinematic quantities. It can be shown that the most general (parity conserving) Lorentz-invariant expression for the cross section for ep \rightarrow eX inelastic scattering, mediated by the exchange of a single virtual photon, is

$$\frac{\mathrm{d}^2 \sigma}{\mathrm{d}x \,\mathrm{d}Q^2} = \frac{4\pi\alpha^2}{Q^4} \left[\left(1 - y - \frac{m_\mathrm{p}^2 y^2}{Q^2} \right) \frac{F_2(x, Q^2)}{x} + y^2 F_1(x, Q^2) \right]. \tag{8.11}$$

Here the functions $f_1(Q^2)$ and $f_2(Q^2)$ of (8.10) have been replaced by the two structure functions, $F_1(x, Q^2)$ and $F_2(x, Q^2)$, where $F_1(x, Q^2)$ can be identified as being purely magnetic in origin. Because the structure functions depend on both Q^2 and x, they cannot be interpreted as the Fourier transforms of the proton charge and magnetic moment distributions; as we will see shortly they represent something more fundamental.

For deep inelastic scattering, where $Q^2 \gg m_{\rm p}^2 y^2$, Equation (8.11) reduces to

$$\frac{\mathrm{d}^2 \sigma}{\mathrm{d}x \,\mathrm{d}Q^2} \approx \frac{4\pi\alpha^2}{Q^4} \left[(1-y) \, \frac{F_2(x,Q^2)}{x} + y^2 F_1(x,Q^2) \right]. \tag{8.12}$$

In fixed-target electron-proton deep inelastic scattering experiments, the Lorentz-invariant kinematic variables Q^2 , x and y can be obtained on an event-by-event basis from the observed energy and scattering angle of the electron, E_3 and θ ,

$$Q^2 = 4E_1E_3\sin^2\frac{\theta}{2}$$
, $x = \frac{Q^2}{2m_p(E_1 - E_3)}$ and $y = 1 - \frac{E_3}{E_1}$,

where E_1 is the incident electron energy. The double-differential cross section is measured by counting the numbers of events in the range $x \to x + \Delta x$ and $Q^2 \to Q^2 + \Delta Q^2$. The double-differential cross section at a particular value of x and Q^2 can be determined for a range of y values, obtained by varying the incident electron energy (see Problem 8.3). The y-dependence of the measured cross sections is then used to disentangle the contributions from $F_1(x, Q^2)$ and $F_2(x, Q^2)$, in much the same way as for the determination of $G_E(Q^2)$ and $G_M(Q^2)$ as described in Section 7.5.1.

Bjorken scaling and the Callan–Gross relation

The first systematic studies of structure functions in inelastic electron–proton scattering were obtained in a series of experiments at the Stanford Linear Accelerator Center (SLAC) in California. Electrons of energies between 5 GeV and 20 GeV were fired at a liquid hydrogen target. The scattering angle of the electron was measured using a large movable spectrometer, in which the energy of the detected final-state electrons could be selected by using a magnetic field. The differential cross sections, measured over a range of incident electron energies, were used to determine the structure functions. The experimental data revealed two striking features, shown in Figure 8.4. The first observation, known as *Bjorken scaling*, was that both $F_1(x, Q^2)$ and $F_2(x, Q^2)$ are (almost) independent of Q^2 , allowing the structure functions to be written as

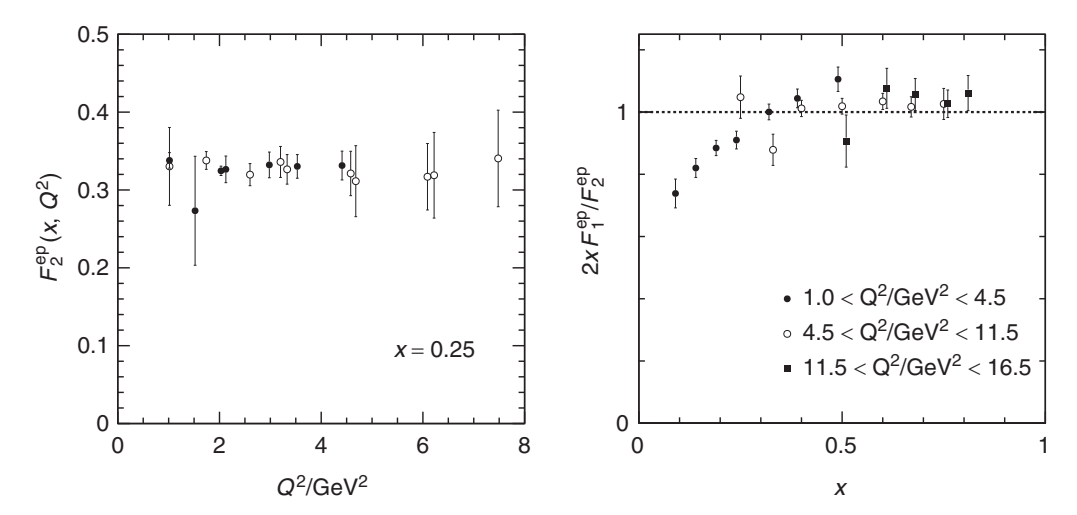
$$F_1(x, Q^2) \to F_1(x)$$
 and $F_2(x, Q^2) \to F_2(x)$.

The lack of Q^2 dependence of the structure functions is strongly suggestive of scattering from point-like constituents within the proton.

The second observation was that in the deep inelastic scattering regime, Q^2 greater than a few GeV², the structure functions $F_1(x)$ and $F_2(x)$ are not independent, but satisfy the *Callan–Gross relation*

$$F_2(x) = 2xF_1(x).$$

This observation can be explained by assuming that the underlying process in electron–proton inelastic scattering is the *elastic* scattering of electrons from point-like *spin-half* constituent particles within the proton, namely the quarks. In this case the electric and magnetic contributions to the scattering process are related by the fixed magnetic moment of a Dirac particle.



Early structure function measurements from fixed-target electron—proton inelastic scattering at SLAC. Left: measurements of $F_2(x, Q^2)$ showing Bjorken scaling. Right: measurements of $2xF_1/F_2$ showing the Callan—Gross relation. Adapted from Friedman and Kendall (1972) and Bodek *et al.* (1979).

8.3 Electron-quark scattering

In the quark model, the underlying interaction in deep inelastic scattering is the QED process of $e^-q \rightarrow e^-q$ elastic scattering and the deep inelastic scattering cross sections are related to the cross section for this quark-level process. The matrix element for $e^-q \rightarrow e^-q$ scattering is obtained from the QED Feynman rules for the Feynman diagram of Figure 8.5. The electron and quark currents are

$$\overline{u}(p_3)[ie\gamma^{\mu}]u(p_1)$$
 and $\overline{u}(p_4)[-iQ_qe\gamma^{\nu}]u(p_2)$,

and the photon propagator is given by $-ig_{\mu\nu}/q^2$ where $q^2=p_1-p_3$. Hence the matrix element can be written

$$\mathcal{M}_{fi} = \frac{Q_{\mathbf{q}}e^2}{q^2} \left[\overline{u}(p_3) \gamma^{\mu} u(p_1) \right] g_{\mu\nu} \left[\overline{u}(p_4) \gamma^{\nu} u(p_2) \right]. \tag{8.13}$$

The spin-averaged matrix element squared can be obtained from the helicity amplitudes (see Problem 6.7), or using the trace approach as described in Section 6.5.5. In either case, in the limit where the electron and quark masses can be neglected, the spin-averaged matrix element squared is given by (6.68),

$$\langle |\mathcal{M}_{fi}|^2 \rangle = 2Q_q^2 e^4 \left(\frac{s^2 + u^2}{t^2} \right) = 2Q_q^2 e^4 \frac{(p_1 \cdot p_2)^2 + (p_1 \cdot p_4)^2}{(p_1 \cdot p_3)^2},$$
 (8.14)

where as usual, $s = p_1 + p_2$, $t = p_1 - p_3$ and $u = p_1 - p_4$.

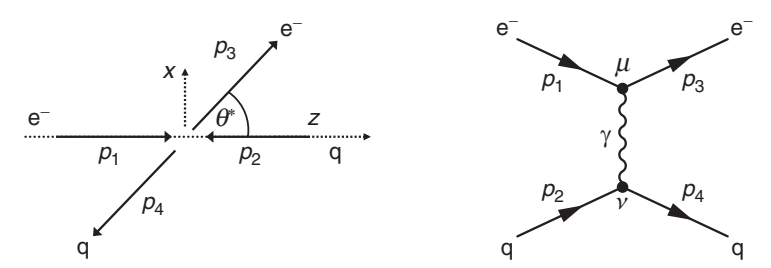


Fig. 8.5 Electron—quark scattering in the centre-of-mass frame and the corresponding lowest-order Feynman diagram.

Here it is convenient to work in the centre-of-mass frame and to express the Lorentz-invariant matrix element of (8.14) in terms of the electron scattering angle, θ^* , as shown in Figure 8.5. Writing the energy of the electron in the centre-of-mass frame as $E = \sqrt{s}/2$, and neglecting the electron and quark masses, the four-momenta of the initial- and final-state particles are given by

$$p_1 = (E, 0, 0, +E),$$
 $p_3 = (E, +E\sin\theta^*, 0, +E\cos\theta^*),$
 $p_2 = (E, 0, 0, -E),$ $p_4 = (E, -E\sin\theta^*, 0, -E\cos\theta^*).$

The four-vector scalar products appearing in (8.14) are

$$p_1 \cdot p_2 = 2E^2$$
, $p_1 \cdot p_3 = E^2(1 - \cos \theta^*)$ and $p_1 \cdot p_4 = E^2(1 + \cos \theta^*)$.

Hence the spin-averaged matrix element squared for the QED process $e^-q \rightarrow e^-q$ is

$$\langle |M_{fi}|^2 \rangle = 2Q_{\rm q}^2 e^4 \frac{4E^4 + E^4 (1 + \cos \theta^*)^2}{E^4 (1 - \cos \theta^*)^2} \ .$$

The differential cross section is obtained by substituting this expression for $\langle |\mathcal{M}_{fi}|^2 \rangle$ into the cross section formula of (3.50), giving

$$\frac{d\sigma}{d\Omega^*} = \frac{Q_q^2 e^4}{8\pi^2 s} \frac{\left[1 + \frac{1}{4} (1 + \cos \theta^*)^2\right]}{(1 - \cos \theta^*)^2}.$$
 (8.15)

The angular dependence in the numerator of (8.15),

$$1 + \frac{1}{4}(1 + \cos \theta^*)^2, \tag{8.16}$$

reflects the chiral structure of the QED interaction. From the arguments of Section 6.4.2, helicity is conserved in the ultra-relativistic limit of the QED interaction. Therefore, the only non-zero matrix elements originate from spin states where the helicities of the electron and the quark are unchanged in the interaction,

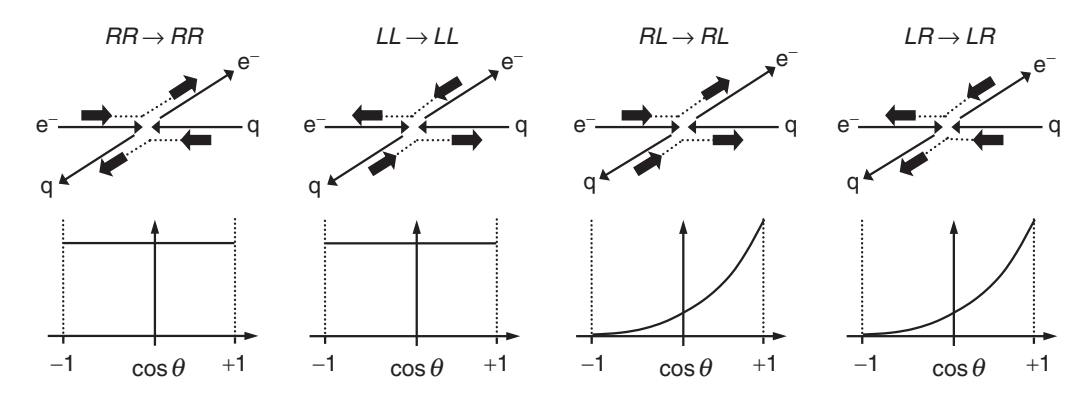


Fig. 8.6 The four helicity combinations contributing to the process $e^-q \to e^-q$ in the limit where $E \gg m$. The first two, $RR \to RR$ and $LL \to LL$, occur in a total spin state with $S_Z = 0$. The second two, $RL \to RL$ and $LR \to LR$, take place in $S_Z = \pm 1$ states.

as shown in Figure 8.6. The $RR \to RR$ and $LL \to LL$ scattering processes occur in a $S_z = 0$ state, where there is no component of the angular momentum in the z-direction. Consequently, there is no preferred polar angle, accounting for the constant term in (8.16). The $RL \to RL$ and $LR \to LR$ scattering processes occur in $S_z = \pm 1$ states and hence (see Section 6.3) result in an angular dependence of

$$\frac{1}{4}(1+\cos\theta^*)^2,$$

explaining the second term in (8.16). The denominator in the expression for the differential cross section of (8.15) arises from the $1/q^2$ propagator term with

$$q^2 = t = (p_1 - p_3)^2 \approx -E^2(1 - \cos \theta^*).$$

When $q^2 \to 0$, in which case the scattering angle $\theta^* \to 0$, the differential cross section tends to infinity. This should not be a surprise. It is analogous to the scattering of a particle in a 1/r potential in classical dynamics; regardless of the impact parameter, there is always a finite deflection (however small). The presence of the propagator term implies that in the QED elastic scattering process, the electron is predominantly scattered in the forward direction.

Lorentz-invariant form

Equation (8.15) gives the $e^-q \rightarrow e^-q$ differential cross section in terms of the centre-of-mass scattering angle θ^* . This can be expressed in a Lorentz-invariant form by writing $\cos \theta^*$ in terms of s and q^2 and changing variables using

$$\frac{\mathrm{d}\sigma}{\mathrm{d}q^2} = \frac{\mathrm{d}\sigma}{\mathrm{d}\Omega^*} \left| \frac{\mathrm{d}\Omega^*}{\mathrm{d}q^2} \right|.$$

Alternatively, the spin-averaged matrix element squared of (8.14) can be substituted directly into the Lorentz-invariant form for the differential cross section of (3.37) with $t = q^2$, giving

$$\frac{d\sigma}{dq^2} = \frac{1}{64\pi s \, p_i^{*2}} \langle |\mathcal{M}_{fi}|^2 \rangle = \frac{Q_q^2 e^4}{32\pi s \, p_i^{*2}} \left(\frac{s^2 + u^2}{t^2} \right). \tag{8.17}$$

Since $p_i^* = \sqrt{s/2}$ and $t = q^2$, Equation (8.17) can be written as

$$\frac{d\sigma}{dq^2} = \frac{Q_q^2 e^4}{8\pi q^4} \left(\frac{s^2 + u^2}{s^2} \right) = \frac{Q_q^2 e^4}{8\pi q^4} \left[1 + \left(\frac{u}{s} \right)^2 \right]. \tag{8.18}$$

Finally, this equation can be expressed in terms of q^2 and s alone by recalling that the sum of the Mandelstam variables s + t + u is equal to the sum of the masses of the initial- and final-state particles. Therefore, in the high-energy limit where the electron and quark masses can neglected,

$$u \approx -s - t = -s - q^2,$$

and the differential cross section for the $e^-q \rightarrow e^-q$ elastic scattering process of (8.18), expressed in terms of s and q^2 alone, is

$$\frac{\mathrm{d}\sigma}{\mathrm{d}q^2} = \frac{2\pi\alpha^2 Q_{\mathrm{q}}^2}{q^4} \left[1 + \left(1 + \frac{q^2}{s} \right)^2 \right]. \tag{8.19}$$

8.4 The quark-parton model

Before quarks and gluons were generally accepted, Feynman proposed that the proton was made up of point-like constituents, termed *partons*. In the quark–parton model, the basic interaction in deep inelastic electron–proton scattering is *elastic* scattering from a spin-half quark within the proton, as shown in Figure 8.7. In this process, the quark is treated as a free particle; this assumption will be justified in Chapter 10. The quark–parton model for deep inelastic scattering is formulated in a frame where the proton has very high energy, $E \gg m_{\rm p}$, referred to as the *infinite momentum frame*. In the infinite momentum frame the mass of the proton can be neglected, such that its four-momentum can be written $p_2 = (E_2, 0, 0, E_2)$. Furthermore, in this frame any component of the momentum of the struck quark transverse to the direction of motion of the proton also can be neglected. Hence, in the infinite momentum frame, the four-momentum of the struck quark can be written

$$p_{\rm q} = \xi p_2 = (\xi E_2, 0, 0, \xi E_2),$$

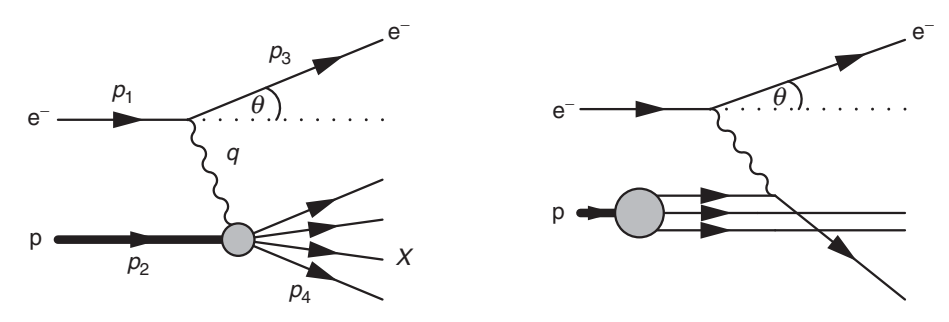


Fig. 8.7 Electron—quark scattering in the centre-of-mass frame and the corresponding lowest-order Feynman diagram.

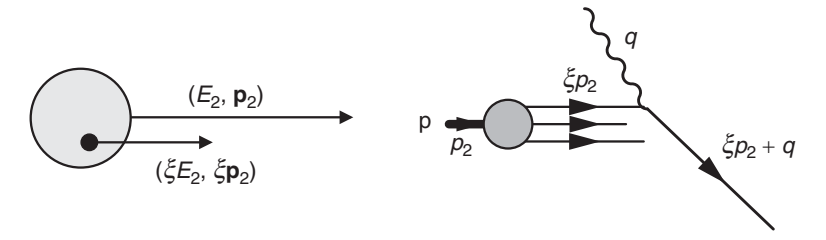


Fig. 8.8 The quark—parton model description of inelastic scattering in terms of the QED interaction between a virtual photon and a quark with the fraction \mathcal{E} of the momentum of the proton.

where ξ is the fraction of momentum of proton carried by the quark, as indicated by Figure 8.8.

The four-momentum of the quark after the interaction with the virtual photon is simply $\xi p_2 + q$. Since the four-momentum squared of the final-state quark is just the square of its mass,

$$(\xi p_2 + q)^2 = \xi^2 p_2^2 + 2\xi p_2 \cdot q + q^2 = m_q^2.$$
 (8.20)

However, ξp_2 is the just four-momentum of the quark before the interaction and therefore $\xi^2 p_2^2 = m_{\rm q}^2$. Thus, (8.20) implies that $q^2 + 2\xi p_2 \cdot q = 0$ and the momentum fraction ξ can be identified as

$$\xi = \frac{-q^2}{2p_2 \cdot q} = \frac{Q^2}{2p_2 \cdot q} \equiv x.$$

Hence, in the quark-parton model, Bjorken x can be identified as the fraction of the momentum of the proton carried by the struck quark (in a frame where the proton has energy $E \gg m_{\rm p}$). Therefore, the measurements of the x-dependence of the structure functions can be related to the momentum distribution of the quarks within the proton.

The kinematic variables for the underlying electron–quark scattering process can be related to those for the electron–proton collision. Neglecting the electron and proton mass terms, the centre-of-mass energy of the e⁻p initial state is

$$s = (p_1 + p_2)^2 \approx 2p_1 \cdot p_2.$$

Because the four-momentum of the struck quark is $p_q = xp_2$, the centre-of-mass energy of the initial-state e^-q system is

$$s_{q} = (p_1 + xp_2)^2 \approx 2xp_1 \cdot p_2 = xs.$$

The kinematic variables x and y, defined in terms of the four-momentum of the proton, are

$$y = \frac{p_2 \cdot q}{p_2 \cdot p_1} \quad \text{and} \quad x = \frac{Q^2}{2p_2 \cdot q}.$$

Similarly, for the electron–quark system,

$$y_{\mathbf{q}} = \frac{p_{\mathbf{q}} \cdot q}{p_{\mathbf{q}} \cdot p_1} = \frac{x p_2 \cdot q}{x p_2 \cdot p_1} = y.$$

Finally, because the underlying electron–quark interaction is an elastic scattering process, $x_q = 1$. Hence, the kinematic variables for the e⁻q interaction are related to those defined in terms of the e⁻p interaction by

$$s_q = xs$$
, $y_q = y$ and $x_q = 1$,

where s, x and y are defined in terms of the electron and proton four-momenta.

The cross section for $e^-q \rightarrow e^-q$ scattering, given by (8.19), can now be written

$$\frac{d\sigma}{dq^2} = \frac{2\pi\alpha^2 Q_q^2}{q^4} \left[1 + \left(1 + \frac{q^2}{s_q} \right)^2 \right],$$
 (8.21)

where s_q is the electron–quark centre-of-mass energy squared. From (8.8), the four-momentum squared of the virtual photon q^2 can be expressed as

$$q^2 = -Q^2 = -(s_q - m_q^2)x_q y_q$$

which in the limit where the quark mass is neglected gives

$$\frac{q^2}{s_{\mathbf{q}}} = -x_{\mathbf{q}}y_{\mathbf{q}} = -y.$$

Hence, the differential cross section of (8.21) can be written

$$\frac{\mathrm{d}\sigma}{\mathrm{d}q^2} = \frac{2\pi\alpha^2 Q_q^2}{q^4} \left[1 + (1-y)^2 \right].$$

Finally, using $q^2 = -Q^2$ and rearranging the terms in the brackets leads to

$$\frac{d\sigma}{dQ^2} = \frac{4\pi\alpha^2 Q_q^2}{Q^4} \left[(1 - y) + \frac{y^2}{2} \right],$$
 (8.22)

Fig. 8.9

which resembles the form of the deep inelastic scattering cross section expressed in terms of the structure functions, as given by (8.12). Equation (8.22) gives the differential cross section for e^-q elastic scattering where the quark carries a fraction x of the momentum of the proton. Although x does not appear explicitly in this equation, the x dependence is implicit through (8.8) whereby

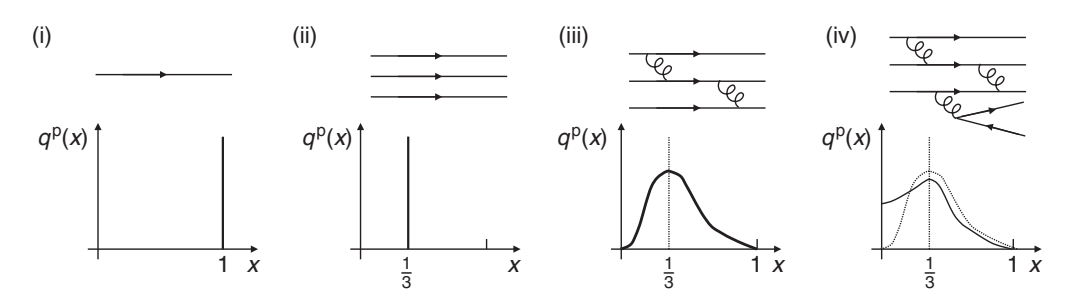
$$y = \frac{Q^2}{(s - m_p^2)x}.$$

8.4.1 Parton distribution functions

The quarks inside the proton will interact with each other through the exchange of gluons. The dynamics of this interacting system will result in a distribution of quark momenta within the proton. These distributions are expressed in terms of *Parton Distribution Functions* (PDFs). For example, the up-quark PDF for the proton $u^p(x)$ is defined such that

$$u^{p}(x) \delta x$$
,

represents the number of up-quarks within the proton with momentum fraction between x and $x + \delta x$. Similarly $d^p(x)$ is the corresponding PDF for the down-quarks. In practice, the functional forms of the PDFs depend on the detailed dynamics of the proton; they are not *a priori* known and have to be obtained from experiment. Figure 8.9 shows a few possible forms of the PDFs that correspond to: (i) the proton consists of a single point-like particle which carries all of the momentum of the proton, in this case the PDF is a Dirac delta-function at x = 1; (ii) the proton consists of three static quarks each of which carries 1/3 of the momentum of the proton, in this case the PDF has the form of a delta-function at x = 1/3 with a normalisation of three; (iii) the three quarks interact with each other and the delta-function at x = 1/3 is smeared out as the quarks exchange momentum; and (iv) higher-order processes, such as virtual quark pairs being produced from gluons



Four possible forms of the quark PDFs within a proton: (i) a single point-like particle; (ii) three static quarks each sharing 1/3 of the momentum of the proton; (iii) three interacting quarks which can exchange momentum; and (iv) interacting quarks including higher-order diagrams. After Halzen and Martin (1984).

inside the proton, tend to result in an enhancement of the PDFs at low x, reflecting the $1/q^2$ nature of the gluon propagator.

The electron–proton deep inelastic scattering cross section can be obtained from the definition of the parton distribution functions and the expression for the differential cross section for underlying electron–quark elastic scattering process given in (8.22). The cross section for elastic scattering from a particular flavour of quark i with charge Q_i and momentum fraction in the range $x \to x + \delta x$, is

$$\frac{\mathrm{d}^2 \sigma}{\mathrm{d} Q^2} = \frac{4\pi\alpha^2}{Q^4} \left[(1-y) + \frac{y^2}{2} \right] \times Q_i^2 q_i^{\mathrm{p}}(x) \,\delta x \,,$$

where $q_i^p(x)$ is the PDF for that flavour of quark. The double-differential cross section is obtained by dividing by δx and summing over all quark flavours

$$\frac{d^2 \sigma^{ep}}{dx \, dQ^2} = \frac{4\pi\alpha^2}{Q^4} \left[(1-y) + \frac{y^2}{2} \right] \sum_i Q_i^2 q_i^p(x).$$
 (8.23)

This is the parton model prediction for the electron–proton deep inelastic scattering cross section. Comparison with (8.12), which is the general expression for the deep inelastic scattering cross section in terms of the structure functions,

$$\frac{\mathrm{d}^2 \sigma}{\mathrm{d}x \mathrm{d}Q^2} = \frac{4\pi \alpha^2}{Q^4} \left[(1 - y) \frac{F_2^{\mathrm{ep}}(x, Q^2)}{x} + y^2 F_1^{\mathrm{ep}}(x, Q^2) \right],$$

leads to the parton model predictions for $F_1^{ep}(x, Q^2)$ and $F_2^{ep}(x, Q^2)$,

$$F_2^{\text{ep}}(x, Q^2) = 2x F_1^{\text{ep}}(x, Q^2) = x \sum_i Q_i^2 q_i^{\text{p}}(x).$$

The parton model naturally predicts Bjorken scaling; because the underlying process is elastic scattering from *point-like* quarks, no (strong) Q^2 dependence is expected. Consequently, both F_1 and F_2 can be written as functions of x alone, $F_1(x,Q^2) \to F_1(x)$ and $F_2(x,Q^2) \to F_2(x)$. The parton model also predicts the Callan–Gross relation, $F_2(x) = 2xF_1(x)$. This is due to the underlying process being elastic scattering from spin-half Dirac particles; the quark magnetic moment is directly related to its charge and therefore the contributions from the electromagnetic (F_2) and the pure magnetic (F_1) structure functions are fixed with respect to one another.

8.4.2 Determination of the parton distribution functions

The parton distribution functions reflect the underlying structure of the proton. At present they cannot be calculated from first principles. This is because the theory of QCD has a large coupling constant, $\alpha_S \sim O(1)$, and perturbation theory cannot

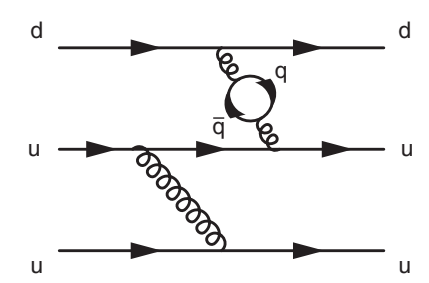


Fig. 8.10 Production of virtual $q\bar{q}$ pairs within the proton.

be applied. The PDFs therefore have to be extracted from measurements of the structure functions in deep inelastic scattering experiments and elsewhere.

For electron–proton deep inelastic scattering, the structure function $F_2^{ep}(x)$ is related to the PDFs by

$$F_2^{\text{ep}}(x) = x \sum_i Q_i^2 q_i^{\text{p}}(x)$$
. (8.24)

In the static model of the proton, it is formed from two up-quarks and a down-quark, and it might be expected that only up- and down-quark PDFs would appear in this sum. However, in reality the proton is a dynamic system where the strongly interacting quarks are constantly exchanging virtual gluons that can fluctuate into virtual $q\bar{q}$ pairs through processes such as that shown in Figure 8.10. Because gluons with large momenta are suppressed by the $1/q^2$ gluon propagator, this *sea* of virtual quarks and antiquarks tend to be produced at low values of x. Electron-proton inelastic scattering therefore involves interactions with both quarks and antiquarks. Furthermore, there will be contributions to the scattering process from strange quarks through interactions with virtual $s\bar{s}$ pairs and even very small contributions from off-mass shell heavier quarks. Here, for the sake of clarity, the relatively small contribution from strange quarks is neglected and the sum in (8.24) is restricted to the light flavours, giving the quark–parton model prediction

$$F_2^{\text{ep}}(x) = x \sum_i Q_i^2 q_i^{\text{p}}(x) \approx x \left(\frac{4}{9} u^{\text{p}}(x) + \frac{1}{9} d^{\text{p}}(x) + \frac{4}{9} \overline{u}^{\text{p}}(x) + \frac{1}{9} \overline{d}^{\text{p}}(x) \right), \quad (8.25)$$

where $u^p(x)$, $d^p(x)$, $\overline{u}^p(x)$ and $\overline{d}^p(x)$ are respectively the up-, down-, anti-up and anti-down parton distribution functions for the proton. A similar expression can be written down for the structure functions for electron–neutron scattering,

$$F_2^{\text{en}}(x) = x \sum_i Q_i^2 q_i^{\text{n}}(x) \approx x \left(\frac{4}{9} u^{\text{n}}(x) + \frac{1}{9} d^{\text{n}}(x) + \frac{4}{9} \overline{u}^{\text{n}}(x) + \frac{1}{9} \overline{d}^{\text{n}}(x) \right), \tag{8.26}$$

where the PDFs now refer to the momentum distributions within the neutron.

With the exception of the relatively small difference in Coulomb interactions between the constituent quarks, the neutron (ddu) would be expected to have the same structure as the proton (uud) with the up- and down-quarks interchanged. This assumed *isospin symmetry* (see Chapter 9) implies that the down-quark PDF in the neutron is the same as the up-quark PDF in the proton and thus

$$d^{\mathbf{n}}(x) = u^{\mathbf{p}}(x)$$
 and $u^{\mathbf{n}}(x) = d^{\mathbf{p}}(x)$.

In order to simplify the notation, the PDFs for the *proton* are usually written as u(x), d(x), $\overline{u}(x)$ and $\overline{d}(x)$, in which case the neutron PDFs can be taken to be

$$d^{n}(x) = u^{p}(x) \equiv u(x)$$
 and $u^{n}(x) = d^{p}(x) \equiv d(x)$.

Likewise, the assumed isospin symmetry implies that the neutron antiquark PDFs can be written in terms of the antiquark PDFs of the proton,

$$\overline{d}^{n}(x) = \overline{u}^{p}(x) \equiv \overline{u}(x)$$
 and $\overline{u}^{n}(x) = \overline{d}^{p}(x) \equiv \overline{d}(x)$.

Thus the proton and neutron structure functions of (8.25) and (8.26), can be written in terms of the PDFs of the proton,

$$F_2^{\text{ep}}(x) = 2xF_1^{\text{ep}}(x) = x\left(\frac{4}{9}u(x) + \frac{1}{9}d(x) + \frac{4}{9}\overline{u}(x) + \frac{1}{9}\overline{d}(x)\right),\tag{8.27}$$

$$F_2^{\text{en}}(x) = 2xF_1^{\text{en}}(x) = x\left(\frac{4}{9}d(x) + \frac{1}{9}u(x) + \frac{4}{9}\overline{d}(x) + \frac{1}{9}\overline{u}(x)\right). \tag{8.28}$$

Integrating these expressions for the structure functions over the entire x range gives

$$\int_0^1 F_2^{\text{ep}}(x) \, \mathrm{d}x = \frac{4}{9} f_{\text{u}} + \frac{1}{9} f_{\text{d}} \quad \text{and} \quad \int_0^1 F_2^{\text{en}}(x) \, \mathrm{d}x = \frac{4}{9} f_{\text{d}} + \frac{1}{9} f_{\text{u}}, \tag{8.29}$$

where $f_{\rm u}$ and $f_{\rm d}$ are defined by

$$f_{\rm u} = \int_0^1 \left[x u(x) + x \overline{u}(x) \right] \mathrm{d}x$$
 and $f_{\rm d} = \int_0^1 \left[x d(x) + x \overline{d}(x) \right] \mathrm{d}x$.

The quantity $f_{\rm u}$ is the fraction of the momentum of the proton carried by the up- and anti-up quarks. Similarly $f_{\rm d}$ is the fraction carried by the down-/anti-down-quarks. The momentum fractions $f_{\rm u}$ and $f_{\rm d}$ can be obtained directly from the experimental measurements of the proton and neutron structure functions. For example, Figure 8.11 shows an experimental measurement of $F_2^{\rm ep}(x,Q^2)$ as a function of x for deep inelastic scattering events with $2\,{\rm GeV}^2 < Q^2 < 30\,{\rm GeV}^2$ as observed at SLAC. The area defined by the measured data points gives

$$\int F_2^{\rm ep}(x) \, \mathrm{d}x \approx 0.18 \, .$$

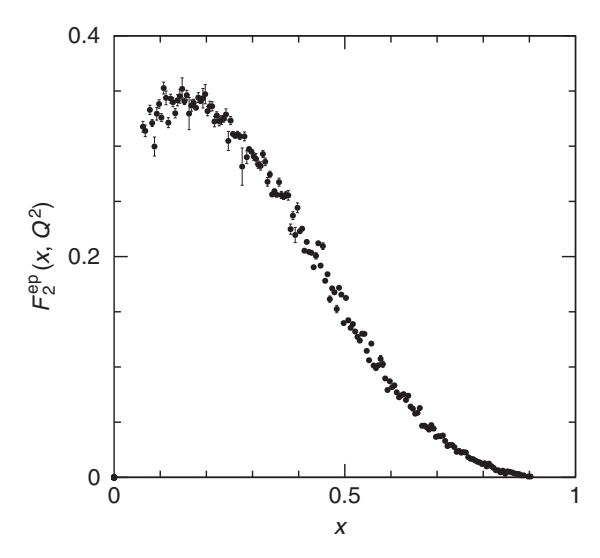


Fig. 8.11 SLAC measurements of $F_2^{ep}(x, Q^2)$ for $2 < Q^2/\text{ GeV}^2 < 30$. Data from Whitlow et al. (1992).

Similarly, $F_2^{\text{en}}(x)$ can be extracted from electron–deuterium scattering data (see Problem 8.6), and it is found that

$$\int F_2^{\rm en}(x) \, \mathrm{d}x \approx 0.12 \, .$$

Using the quark–parton model predictions of (8.29), these experimental results can be interpreted as measurements of the fractions of the momentum of the proton carried by the up-/anti-up- and down-/anti-down-quarks:

$$f_{\rm u} \approx 0.36$$
 and $f_{\rm d} \approx 0.18$.

Given that the proton consists of two up-quarks and one down-quark, it is perhaps not surprising that $f_{\rm u}=2f_{\rm d}$. Nevertheless, the total fraction of the momentum of the proton carried by quarks and antiquarks is just over 50%; the remainder is carried by the gluons that are the force carrying particles of the strong interaction. Because the gluons are electrically neutral, they do not contribute to the QED process of electron–proton deep inelastic scattering.

8.4.3 Valence and sea quarks

It is already clear that the proton is a lot more complex than first might have been anticipated. The picture of a proton as a bound state consisting of three "valence" quarks is overly simplistic. The proton not only contains quarks, but also contains of a sea of virtual gluons that give rise to an antiquark component through $g \to q\bar{q}$ pair production. To reflect these two distinct components, the up-quark PDF can be split into the contribution from the two valence quarks, written as $u_V(x)$, and a

contribution from the *sea* of up-quarks that are pair-produced from virtual gluons, $u_S(x)$. In this way, the proton light quark PDFs can be decomposed into

$$u(x) = u_{V}(x) + u_{S}(x)$$
 and $d(x) = d_{V}(x) + d_{S}(x)$.

In the case of the antiquark PDFs, there are only sea quark contributions,

$$\overline{u}(x) \equiv \overline{u}_{S}(x)$$
 and $\overline{d}(x) \equiv \overline{d}_{S}(x)$.

Since the proton consists of two valence up-quarks and one valence down-quark, it is reasonable to expect that the valence quark PDFs are normalised accordingly,

$$\int_0^1 u_{\rm V}(x) \, dx = 2 \quad \text{and} \quad \int_0^1 d_{\rm V}(x) \, dx = 1.$$

Although there is no corresponding *a priori* expectation for the sea quarks, some reasonable assumptions can be made. Firstly, since the sea quarks and the antiquarks of a given flavour are produced in pairs, the sea quark PDF will be the same as the PDF for the corresponding antiquark. Furthermore, since the masses of the up- and down-quarks are similar, it is reasonable to expect that the sea PDFs for the up- and down-quarks will be approximately the same. With these assumptions, the sea PDFs can all be approximated by a single function, written S(x), such that

$$u_{\rm S}(x) = \overline{u}_{\rm S}(x) \approx d_{\rm S}(x) = \overline{d}_{\rm S}(x) \approx S(x).$$

Writing (8.27) and (8.28) in terms of the valence and sea quark PDFs leads to

$$F_2^{\text{ep}}(x) = x \left(\frac{4}{9} u_{\text{V}}(x) + \frac{1}{9} d_{\text{V}}(x) + \frac{10}{9} S(x) \right),$$

$$F_2^{\text{en}}(x) = x \left(\frac{4}{9} d_{\text{V}}(x) + \frac{1}{9} u_{\text{V}}(x) + \frac{10}{9} S(x) \right).$$

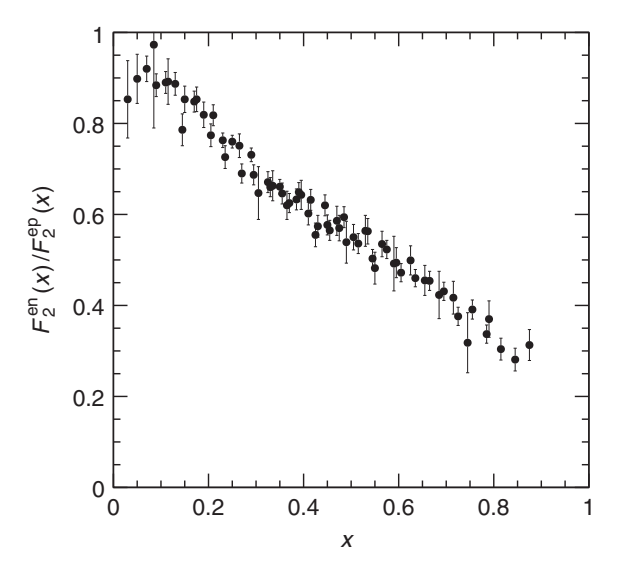
With the above assumptions, the ratio of $F_2^{en}(x)$ to $F_2^{ep}(x)$ is predicted to be

$$\frac{F_2^{\text{en}}(x)}{F_2^{\text{ep}}(x)} = \frac{4d_{\text{V}}(x) + u_{\text{V}}(x) + 10S(x)}{4u_{\text{V}}(x) + d_{\text{V}}(x) + 10S(x)}.$$
(8.30)

Although the PDFs need to be determined experimentally, some qualitative predictions can be made. For example, since the sea quarks are expected to be produced mainly at low x, it is reasonable to hypothesise that the sea quarks will give the dominant contribution to the proton PDFs at low x. In this case, the low-x limit of (8.30) would be

$$\frac{F_2^{\text{en}}(x)}{F_2^{\text{ep}}(x)} \to 1 \quad \text{as } x \to 0.$$

This prediction is supported by the data of Figure 8.12, which shows the ratio of the $F_2^{\rm en}(x)/F_2^{\rm ep}(x)$ obtained from electron–proton and electron–deuterium deep inelastic scattering measurements.



The ratio of $F_2^{\text{en}}(x)/F_2^{\text{ep}}(x)$ obtained from electron—deuterium and electron—proton deep inelastic scattering measurements at SLAC. Data from Bodek *et al.* (1979).

Owing to the $1/q^2$ gluon propagator, which will suppress the production of sea quarks at high x, it might be expected that the high-x PDFs of the proton will be dominated by the valence quarks. In this case,

$$\frac{F_2^{\text{en}}(x)}{F_2^{\text{ep}}(x)} \to \frac{4d_{\text{V}}(x) + u_{\text{V}}(x)}{4u_{\text{V}}(x) + d_{\text{V}}(x)}$$
 as $x \to 1$.

If it is also assumed that $u_V(x) = 2d_V(x)$, the ratio of $F_2^{\text{en}}(x)/F_2^{\text{ep}}(x)$ would be expected to tend to 2/3 as $x \to 1$. This is in clear disagreement with the data of Figure 8.12, where it can be seen that

$$\frac{F_2^{\text{en}}(x)}{F_2^{\text{ep}}(x)} \to \frac{1}{4} \quad \text{as } x \to 1.$$

This would seem to imply that the ratio $d_V(x)/u_V(x) \to 0$ as $x \to 1$. Whilst this behaviour is not fully understood, a qualitative explanation based on the exclusion principle can be made. At high x, one of the valence quarks carries most of the momentum of the proton and the other two valence quarks must be in a low momentum state. Since the exclusion principle forbids two like-flavour quarks being in the same state, the configuration where the down-quark in the proton is at high x and both up-quarks have low momentum is disfavoured.

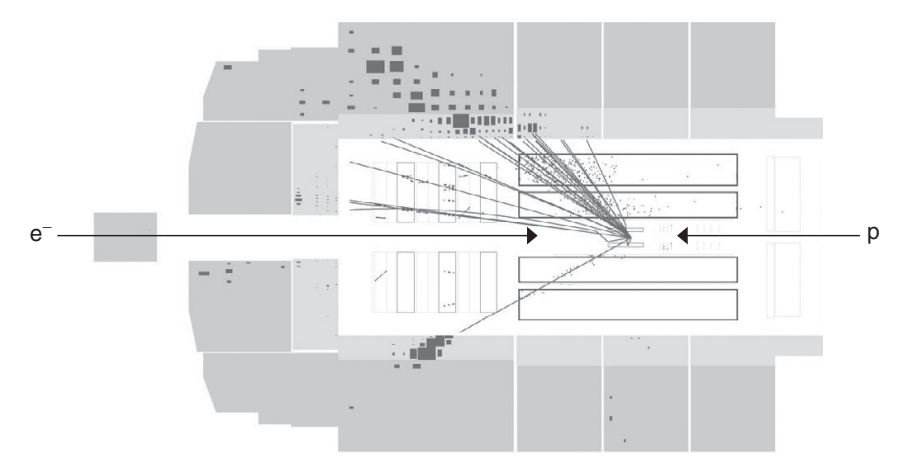
There are a number of conclusions that can be drawn from the above discussion. Firstly, the proton is a complex system consisting of many strongly interacting quarks and gluons. Secondly, whilst qualitative predictions of the properties of the

PDFs can be made, relatively simplistic arguments do not always work. Ultimately, the parton distribution functions have to be inferred directly from experimental data.

8.5 Electron-proton scattering at the HERA collider

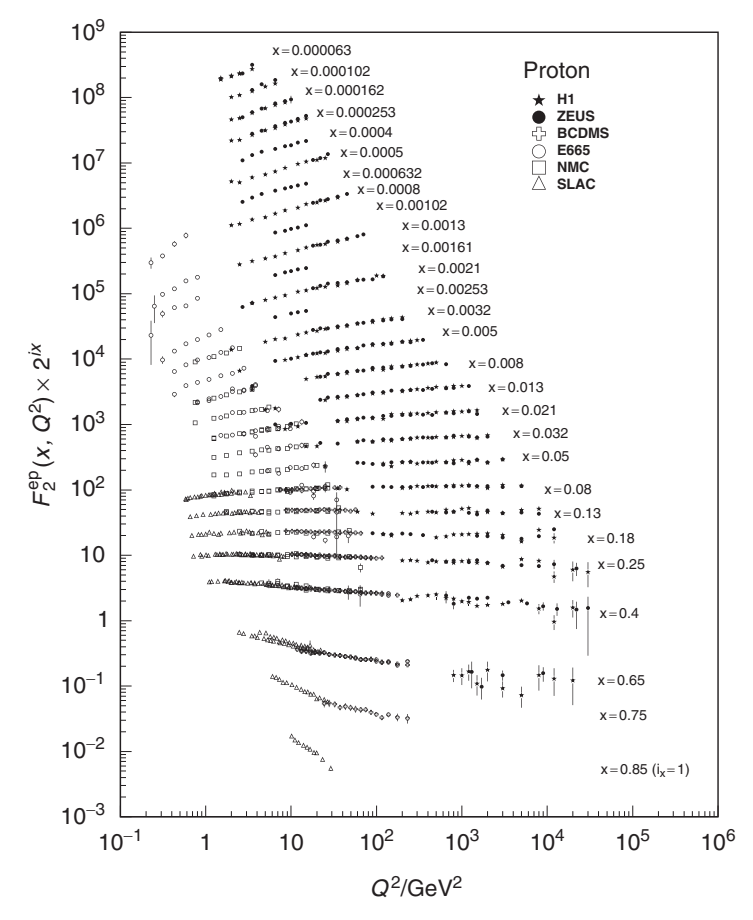
The studies of deep inelastic scattering at very high Q^2 and at very low x were amongst the main goals of the HERA electron–proton collider that operated from 1991 to 2007 at the DESY (Deutsches Elektronen-Synchrotron) laboratory in Hamburg, Germany. It consisted of a 3 km circumference ring where 27.5 GeV electrons (or positrons) were collided with 820 GeV or 920 GeV protons. Two large experiments, H1 and ZEUS, were located at opposite sides of the ring. Each experiment recorded over one million $e^{\pm}p$ deep inelastic collisions at $Q^2 > 200 \,\text{GeV}^2$. These large data samples at a centre-of-mass energy of $\sqrt{s} \approx 300 \,\text{GeV}$, enabled the structure of the proton to be probed with high precision, both at Q^2 values of up to $2 \times 10^4 \,\text{GeV}^2$ and at x below 10^{-4} .

Figure 8.13 shows an example of a very-high- Q^2 interaction recorded by the H1 experiment. The final-state hadronic system is observed as a jet of high-energy particles. The energy and direction of this jet of particles is measured less precisely than the corresponding properties of the electron. Consequently, for each observed event, Q^2 and x are determined from the energy and scattering angle of the electron. The results from deep inelastic scattering data from the H1 and ZEUS experiments, summarised in Figure 8.14, provide a precise determination of the proton structure functions over a very wide range of x and Q^2 . The data show a number



A high-energy electron—proton collision in the H1 detector at HERA. In this event the electron (the particle recorded in the lower part of the detector) is scattered through a large angle and the hadronic system from the break up of the proton forms a jet of particles. Courtesy of the H1 Collaboration.

Fig. 8.13



Measurements of $F_2^{ep}(x, Q^2)$ at HERA. Results from both the H1 and ZEUS experiments are shown. The different bands of data points correspond to the Q^2 evolution of F^{ep} for different values of x. For clarity, the data at different values of x are shifted by $-\log x$. Also shown are lower- Q^2 data from earlier fixed-target experiments (BCDMS, E665, NMC and the SLAC experiments). From Beringer et al. (2012), ©the American Physical Society.

of interesting features. For 0.01 < x < 0.5, where the measurements extend out to $Q^2 = 2 \times 10^4 \,\mathrm{GeV^2}$, only a weak Q^2 dependence of $F_2^{\mathrm{ep}}(x,Q^2)$ is observed, broadly consistent with Bjorken scaling. It can therefore be concluded that quarks appear to be point-like particles at scales of up to $Q^2 = 2 \times 10^4 \,\mathrm{GeV^2}$. If the quark was a composite particle, deviations from Bjorken scaling would be expected when the wavelength of the virtual photon, $\lambda \sim hc/|\mathbf{Q}|$, became comparable to the size of the quark. The observed consistency with Bjorken scaling therefore implies that the radius of a quark must be smaller than

$$r_{\rm q} < 10^{-18} \, \rm m.$$

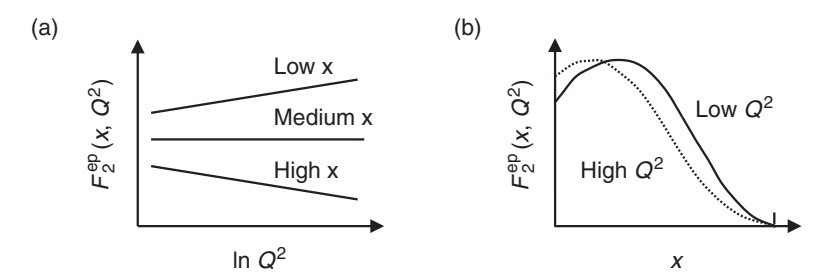
Fig. 8.16

8.5.1 Scaling violations

Whilst Bjorken scaling holds over a wide range of x values, relatively small deviations are observed at very low and very high values of x. For example, at high (low) values of x, the proton structure function is observed to decrease (increase) with increasing Q^2 . Put another way, at high Q^2 the measured structure functions are shifted towards lower values of x relative to the structure functions at low Q^2 , as indicated in Figure 8.15. This behaviour, known as scaling violation, implies that at high Q^2 , the proton is observed to have a greater fraction of low x quarks. These scaling violations are not only expected, but the observed Q^2 dependence is calculable in the theory of the strong interaction, QCD.

The mathematical description of the origin of scaling violations is beyond the scope of this book and only a qualitative description is given here. At low Q^2 , there is a length scale, determined by the wavelength of the virtual photon, below which it is not possible to resolve any spatial sub-structure, as indicated in Figure 8.16a. At higher values of Q^2 , corresponding to shorter-wavelengths of the virtual photon, it is possible to resolve finer detail. In this case, the deep inelastic scattering process is sensitive to the effects of quarks radiating virtual gluons, $q \rightarrow qg$, over smaller length scales, as indicated in Figure 8.16b. Consequently, more low-x quarks are "seen" in high- Q^2 deep inelastic scattering.

Although currently it is not possible to calculate the proton PDFs from first principles within the theory of QCD, the Q^2 dependence of the PDFs is calculable



The general features of the evolution of $F_2^{ep}(x, Q^2)$: (a) the Q^2 dependence at low and high x and (b) the x dependence at low and high Q^2 .



Finer structure within the proton can be resolved by shorter-wavelength virtual photons leading to the observation of lower x partons at higher Q^2 . The circled regions indicate the length scale below which structure cannot be resolved.

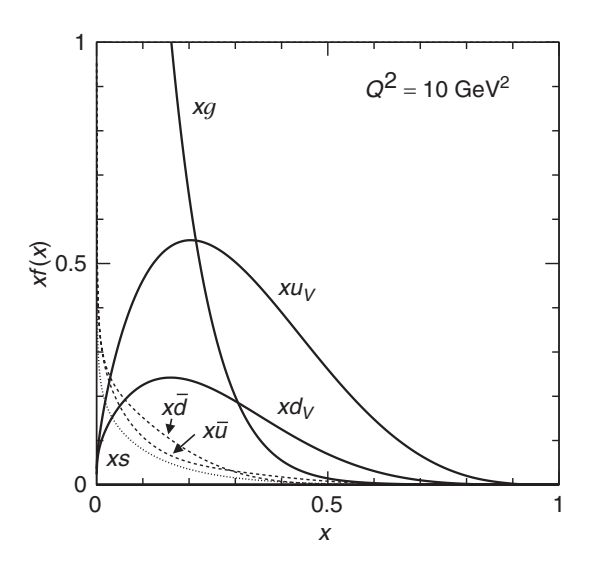
Fig. 8.17

using the parton evolution functions known as the DGLAP (Dokshitzer–Gribov–Lipatov–Altarelli–Parisi) equations. These equations are based on universal parton splitting functions for the QCD processes $q \to qg$ and $g \to q\overline{q}$. The observed scaling violations in deep inelastic scattering therefore provide a powerful validation of the fundamental QCD theory of the strong interaction. A good introduction to the DGLAP evolution equations can be found in Halzen and Martin (1984).

8.6 Parton distribution function measurements

Information about the parton distribution functions of the proton can be extracted from high-energy measurements involving protons, such as: fixed-target electron–proton and electron–neutron scattering; high-energy electron–proton collider data; neutrino–nucleon scattering data (discussed in Chapter 12); high-energy $p\bar{p}$ collider data from the Tevatron; and very-high-energy pp collider data from the LHC. The different experimental measurements provide complementary information about the PDFs. For example, neutrino scattering data provide a direct measurement of the $\bar{u}(x)$ and $\bar{d}(x)$ content of the proton and the pp collider data provides information on the gluon PDF, g(x).

The proton PDFs are extracted from a global fit to a wide range of experimental data. Owing to the complementary nature of the different measurements, tight constraints on the PDFs are obtained. In practice, the PDFs are varied, subject to the



The current understanding of the proton PDFs at $Q^2 = 10 \text{ GeV}^2$ as determined from the MRST fit to a wide range of experimental data. The relatively small strange quark PDF s(x) is shown. PDFs from the Durham HepData project.

203 Summary

constraints imposed by the theoretical framework of QCD such as the DGLAP evolution equations, to obtain the best agreement with experimental data. The output of this procedure is a set of PDFs at a particular Q^2 scale. For example, Figure 8.17 shows the extracted PDFs at $Q^2 = 10 \, \text{GeV}^2$ obtained from a recent fit to the experimental data, where it is assumed that $u(x) = u_V(x) + \overline{u}(x)$. The contribution from gluons is large and, as expected, is peaked towards low values of x. The antiquark PDFs are relatively small and, because the antiquarks originate from $g \to q\overline{q}$, also are peaked towards low values of x. Apart from at high values of x, it is found that $u_V(x) \approx 2d_V(x)$ as expected. Finally, it is worth noting that although the PDFs for \overline{u} and \overline{d} are similar, there is a small difference with $\overline{d}(x) > \overline{u}(x)$. This may be explained by a relative suppression of the $g \to u\overline{u}$ process due to the exclusion principle and the larger number of up-quark states which are already occupied.

Summary

In this chapter the process of deep inelastic scattering has been described in terms of the quark-parton model, where the underlying process is the elastic scattering of the electron from the quasi-free spin-half constituent quarks. The kinematics of inelastic scattering were described in terms of two of the kinematic variables defined below

$$Q^2 \equiv -q^2$$
, $x \equiv \frac{Q^2}{2p_2 \cdot q}$, $y \equiv \frac{p_2 \cdot q}{p_2 \cdot p_1}$ and $v \equiv \frac{p_2 \cdot q}{m_p}$.

In the quark–parton model, x is identified as the fraction of the momentum of the proton carried by the struck quark in the underlying $e^-q \rightarrow e^-q$ elastic scattering process. The quark–parton model naturally describes the experimentally observed phenomena of Bjorken scaling, $F(x, Q^2) \rightarrow F(x)$, and the Callan–Gross relation, $F_2(x) = 2xF_1(x)$.

In the quark–parton model, cross sections can be described in terms of parton distribution functions (PDFs) which represent the momentum distributions of quarks and antiquarks within the proton. The PDFs can not yet be calculated from first principles but are determined from a wide range of experimental data. The resulting PDF measurements reveal the proton to be much more complex than a static bound state of three quarks (uud); it is a dynamic object consisting of three valence quarks and a sea of virtual quarks, antiquarks and gluons, with almost 50% of the momentum of the proton carried by the gluons. The precise knowledge of the PDFs is an essential ingredient to the calculations of cross sections for all high-energy processes involving protons, such as proton–proton collisions at the LHC.

The quark—parton model provides a hugely successful description of the dynamic nature of the proton. However, it does not explain why the only observed hadronic states are baryons and mesons or why the proton is the lowest mass baryon. The static quark model is the subject of the next chapter.

Problems

- **8.1** Use the data in Figure 8.2 to estimate the lifetime of the Δ^+ baryon.
- 8.2 In fixed-target electron–proton *elastic* scattering $Q^2 = 2m_{\rm p}(E_1 E_3) = 2m_{\rm p}E_1 y \quad \text{and} \quad Q^2 = 4E_1E_3\sin^2(\theta/2).$
 - (a) Use these relations to show that

$$\sin^2\left(\frac{\theta}{2}\right) = \frac{E_1}{E_3} \frac{m_{\rm p}^2}{O^2} y^2 \quad \text{and hence} \quad \frac{E_3}{E_1} \cos^2\left(\frac{\theta}{2}\right) = 1 - y - \frac{m_{\rm p}^2 y^2}{O^2}.$$

(b) Assuming azimuthal symmetry and using Equations (7.31) and (7.32), show that

$$\frac{\mathrm{d}\sigma}{\mathrm{d}Q^2} = \left|\frac{\mathrm{d}\Omega}{\mathrm{d}Q^2}\right| \frac{\mathrm{d}\sigma}{\mathrm{d}\Omega} = \frac{\pi}{E_3^2} \frac{\mathrm{d}\sigma}{\mathrm{d}\Omega}.$$

(c) Using the results of (a) and (b) show that the Rosenbluth equation,

$$\frac{\mathrm{d}\sigma}{\mathrm{d}\Omega} = \frac{\alpha^2}{4E_1^2\sin^4(\theta/2)} \frac{E_3}{E_1} \left(\frac{G_E^2 + \tau G_M^2}{(1+\tau)} \cos^2\frac{\theta}{2} + 2\tau G_M^2 \sin^2\frac{\theta}{2} \right),$$

can be written in the Lorentz-invariant form

$$\frac{\mathrm{d}\sigma}{\mathrm{d}Q^2} = \frac{4\pi\alpha^2}{Q^4} \left[\frac{G_E^2 + \tau G_M^2}{(1+\tau)} \left(1 - y - \frac{m_{\rm p}^2 y^2}{Q^2} \right) + \frac{1}{2} y^2 G_M^2 \right].$$

- **8.3** In fixed-target electron—proton inelastic scattering:
 - (a) show that the laboratory frame differential cross section for deep-inelastic scattering is related to the Lorentz-invariant differential cross section of Equation (8.11) by

$$\frac{\mathrm{d}^2 \sigma}{\mathrm{d} E_3 \, \mathrm{d} \Omega} = \frac{E_1 E_3}{\pi} \frac{\mathrm{d}^2 \sigma}{\mathrm{d} E_3 \, \mathrm{d} Q^2} = \frac{E_1 E_3}{\pi} \frac{2 m_\mathrm{p} x^2}{Q^2} \frac{\mathrm{d}^2 \sigma}{\mathrm{d} x \, \mathrm{d} Q^2},$$

where E_1 and E_3 are the energies of the incoming and outgoing electron.

(b) Show that

$$\frac{2m_{\rm p}x^2}{Q^2} \cdot \frac{y^2}{2} = \frac{1}{m_{\rm p}} \frac{E_3}{E_1} \sin^2 \frac{\theta}{2} \quad \text{and} \quad 1 - y - \frac{m_{\rm p}^2 x^2 y^2}{Q^2} = \frac{E_3}{E_1} \cos^2 \frac{\theta}{2}.$$